Cellular/Molecular

Astrocytes Modulate a Postsynaptic NMDA–$GABA_A$-Receptor Crosstalk in Hypothalamic Neurosecretory Neurons

Evgeniy S. Potapenko, Vinicia C. Biancardi, Yiqiang Zhou, and Javier E. Stern
Department of Physiology, Georgia Health Sciences University, Augusta, Georgia 30912

A dynamic balance between the excitatory and inhibitory neurotransmitters glutamate and GABA is critical for maintaining proper neuronal activity in the brain. This balance is partly achieved via presynaptic interactions between glutamatergic and $GABA_A$ergic synapses converging into the same targets. Here, we show that in hypothalamic magnocellular neurosecretory neurons (MNCs), a direct crosstalk between postsynaptic NMDA receptors (NMDARs) and $GABA_A$ receptors ($GABA_A$Rs) contributes to the excitatory/inhibitory balance in this system. We found that activation of NMDARs by endogenous glutamate levels controlled by astrocyte glutamate transporters, evokes a transient and reversible potentiation of postsynaptic $GABA_A$Rs. This inter-receptor crosstalk is calcium-dependent and involves a kinase-dependent phosphorylation mechanism, but does not require nitric oxide as an intermediary signal. Finally, we found the NMDAR–$GABA_A$R crosstalk to be blunted in rats with heart failure, a pathological condition in which the hypothalamic glutamate–GABA balance is tipped toward an excitatory predominance. Together, our findings support a novel form of glutamate–GABA interactions in MNCs, which involves crosstalk between NMDA and $GABA_A$ postsynaptic receptors, whose strength is controlled by the activity of local astrocytes. We propose this inter-receptor crosstalk to act as a compensatory, counterbalancing mechanism to dampen glutamate-mediated overexcitation. Finally, we propose that an uncoupling between NMDARs and $GABA_A$Rs may contribute to exacerbated neuronal activity and, consequently, sympathohumoral activation in such disease conditions as heart failure.

Introduction

A dynamic balance between the excitatory and inhibitory neurotransmitters glutamate and GABA is critical for maintaining neuronal network behavior. Conversely, an altered synaptic balance contributes to inappropriate neuronal activity in pathological states, including Alzheimer's disease, Huntington's disease, and schizophrenia, among others (Kehrer et al., 2008; Cummings et al., 2009; Sun et al., 2009). Maintenance of a proper inhibitory–excitatory balance is in part achieved via direct crosstalk among glutamatergic and GABAergic synapses converging on the same target. Multiple modalities of intersynaptic crosstalk have been described in the CNS. One of the best characterized involves a presynaptic locus, by which spillover of glutamate diffuses locally to activate presynaptic receptors in neighboring GABAergic terminals to influence release probability (i.e., heterosynaptic axo–axonal interactions) (Vogt and Nicoll, 1999; Mitchell and Silver, 2000; Semyanov and Kullmann, 2000). The efficiency of this type of intersynaptic crosstalk is influenced by surrounding astrocytes, which tightly regulate neurotransmitter diffusion in the extracellular space, acting both as a physical barrier, and via the activity of high-affinity glutamate transporters (Piet et al., 2004).

Accumulating evidence indicates that glutamate–GABA intersynaptic crosstalk may also involve a postsynaptic locus, which plays an important role in long-term forms of synaptic plasticity. Thus, long-term depression (Morishita and Sastry, 1996; Wang and Stelzer, 1996; Lu et al., 2000) and long-term potentiation (Kano et al., 1992) of GABAergic synapses in various CNS regions have been shown to involve an NMDAR-dependent change in postsynaptic $GABA_A$-receptor ($GABA_A$R) function.

Whether a postsynaptic NMDA receptor (NMDAR)–$GABA_A$R crosstalk is also involved in short-term forms of GABAergic inhibitory plasticity, whether its activation is under the control of neighboring astrocytes, and whether an altered inter-receptor crosstalk contributes to altered excitatory/inhibitory balance in disease conditions, are important questions that remain unanswered. To address these questions, we used the hypothalamic magnocellular system as an experimental network model. This is a relatively simple and well characterized system comprising neurosecretory vasopressin (VP) and oxytocin neurons in the supraoptic (SON) and paraventricular nuclei. Neuronal firing activity in this nuclei, and thus neurosecretory output from this system (Cazalis et al., 1985), is tightly controlled by glutamate and GABA synaptic inputs, acting most predominantly on postsynaptic NMDARs and $GABA_A$Rs, respectively (Randle and Renaud, 1987; Nissen et al., 1995; Park et al., 2006). Importantly, presynaptic glutamate–GABA interactions, dynamically controlled by surrounding astrocytes, are critical in fine-tuning neuronal

Received Aug. 17, 2012; revised Sept. 27, 2012; accepted Oct. 18, 2012.
Author contributions: E.S.P. and J.E.S. designed research; E.S.P., V.C.B., Y.Z., and J.E.S. performed research; E.S.P., V.C.B., and J.E.S. analyzed data; J.E.S. wrote the paper.
This work was supported by National Heart, Lung, and Blood Institute Grant NIH HL085767 to J.E.S.
The authors declare no competing financial interests.
Correspondence should be addressed to Dr. Javier E. Stern, Department of Physiology, Georgia Health Sciences University, 1120 15th Street, Augusta, GA 30912. E-mail: jstern@georgiahealth.edu.
DOI:10.1523/JNEUROSCI.3936-12.2013
Copyright © 2013 the authors 0270-6474/13/330631-10$15.00/0

output from this system, contributing in turn to activity-dependent homeostatic plastic adjustments during conditions of high hormonal demand (Oliet et al., 2001; Piet et al., 2004).

Our results show that activation of NMDARs by endogenous glutamate levels controlled by astrocyte glutamate transporters, evokes a transient and reversible potentiation of postsynaptic $GABA_A$Rs. This effect is calcium-dependent and involves a kinase-dependent phosphorylation mechanism. Finally, we found a blunted NMDAR–$GABA_A$R crosstalk in heart-failure (HF) rats, a pathological condition in which the glutamate–GABA balance is tipped toward an excitatory predominance. Together, results from this work support a novel form of NMDAR–$GABA_A$R crosstalk in hypothalamic neurons, which may play a critical pathophysiological role in sympathohumoral activation in disease conditions.

Materials and Methods

Animals and induction of HF. Male Wistar rats (150–180 g) were purchased from Harlan Laboratories and housed at room temperature (24−26°C) in a 12 h light/dark cycle room and given *ad libitum* access to food and water. All procedures were performed in agreement with guidelines of the Georgia Health Sciences University Institutional Animal Care and Use Committee. HF was induced by coronary artery ligation as previously described (Biancardi et al., 2011; Potapenko et al., 2011). Briefly, animals were anesthetized with isoflurane 4% and intubated for mechanical ventilation. A left thoracotomy was performed and the heart exteriorized. The ligation was placed on the main diagonal branch of the left anterior descending coronary artery. Buprenorphine (0.3 mg/kg, s.c.; Bruprenex C3, Butler Schein Animal Health) was given immediately after surgery to minimize postsurgical pain. Sham animals underwent the same procedure but the coronary artery was not ligated. All animals were used 6–7 weeks after surgery. Transthoracic echocardiography (Vevo 770 system, VisualSonics) was performed 4 weeks after surgery under light anesthesia. The left ventricle internal diameter, as well as the left diameter of the ventricle posterior and anterior walls, was obtained throughout the cardiac cycle from the short-axis motion imaging mode. Measured parameters were used to calculate ejection fraction and fractional shortening. In a subset of experiments, we also used male heterozygous transgenic AVP-eGFP Wistar rats (5–6 weeks old), in which VP neurons are endogenously fluorescent (Ueta et al., 2005).

Retrograde tracing. Presympathetic rostral ventrolateral medulla (RVLM)-projecting paraventricular nucleus of the hypothalamus (PVN) neurons (PVN-RVLM) were identified by injecting rhodamine beads unilaterally into the brainstem region containing the RVLM as previously described (Sonner et al., 2011). Rats were anesthetized (ketamine–xylazine mixture, 90 and 50 mg/kg^{-1}, respectively, i.p.) and a stereotaxic apparatus was used to pressure inject 500 nl of rhodamine-labeled microspheres (Lumaflor) into the RVLM (starting from bregma, 12 mm caudal along the lamina, 2 mm medial lateral, and 8 mm ventral). In general, RVLM injection sites were contained within the caudal pole of the facial nucleus to ~1 mm more caudal, and were ventrally located with respect to the nucleus ambiguous. The location of the tracer was verified histologically (Sonner et al., 2011). Injections located either more rostral or lateral to the targeted area did not result in PVN labeling, and these animals were discarded from the study. Animals were used 3–4 d after surgery.

Hypothalamic slice preparation. Hypothalamic brain slices were prepared according to methods previously described (Stern, 2001; Potapenko et al., 2011). Briefly, rats were deeply anesthetized with pentobarbital (80 mg/kg^{-1}, i.p.), and perfused through the heart with an ice-cold sucrose solution containing (in mM[SCAP]) the following: 200 sucrose, 2.5 KCl, 3 $MgSO_4$, 26 $NaHCO_3$, 1.25 NaH_2PO_4, 20 D-glucose, 0.4 ascorbic acid, 1 $CaCl_2$, and 2 pyruvic acid (290–310 mosmol l^{-1}). Rats were then quickly decapitated, brains dissected out, and coronal slices cut (300 μm thick) using a vibroslicer (DSK Microslicer, Ted Pella). An oxygenated ice-cold artificial CSF (ACSF) was used during slicing. This ACSF contained (in mM[SCAP]) the following: 119 NaCl, 2.5 KCl, 1 $MgSO_4$, 26 $NaHCO_3$, 1.25 NaH_2PO_4, 20 D-glucose, 0.4 ascorbic acid, 2 $CaCl_2$, and 2 pyruvic acid, pH 7.4; 290–310 mosmol l^{-1}. Slices were placed in a holding chamber containing ACSF and kept at room temperature until used.

Patch-clamp electrophysiology. Slices were bathed with solutions (~2.0 ml/min^{-1}) that were continuously bubbled with 95% O_2-5% CO_2 and maintained at ~32°C. Thin-walled (outer diameter, 1.5 mm; inner diameter, 1.17 mm) borosilicate glass (G150TF-3, Warner Instruments) was used to pull patch pipettes (3–4 MΩ) on a horizontal Flaming/Brown micropipette puller (P-97, Sutter Instruments). The internal solution contained the following (in mM): 140 potassium gluconate, 0.2 EGTA, 10 HEPES, 10 KCl, 0.9 $MgCl_2$, 4 MgATP, 0.3 NaGTP, and 20 phosphocreatine (Na^+), pH 7.2–7.3. A low-Mg^{2+} ACSF (20 μM $MgSO_4$,) was used to facilitate measurements of NMDA-mediated currents. Recordings were obtained with an Axopatch 200B amplifier (Molecular Devices) from SON neurons using infrared differential interference contrast (IR-DIC) videomicroscopy, or from fluorescently labeled PVN-RVLM neurons located in the parvocellular ventromedial subnucleus of the PVN, using a combination of fluorescence illumination and IR-DIC videomicroscopy. The voltage output was digitized at 16 bit resolution, 10 kHz, and was filtered at 2 kHz (Digidata 1320A, Molecular Devices). Data were discarded if the series resistance was not stable throughout the entire recording (>20% change), or if neuronal input resistance was lower than 350 MΩ at the beginning of the recording (Stern, 2001; Potapenko et al., 2011). Focal activation of $GABA_A$Rs was achieved by delivering the $GABA_A$R agonist muscimol with a picospritzer device (Toohey) connected to a patch pipette positioned ~10 μm from the recorded cell. The area of the $GABA_A$-mediated current (I_{GABAA}) was quantified and expressed as charge transfer. The I_{GABAA} current density was determined by dividing the current area by the cell capacitance, which was obtained by integrating the area under the transient capacitive phase of a 5 mV depolarizing step pulse, in voltage-clamp mode.

Miniature $GABA_A$-mediated IPSCs (mIPSCs) were recorded and analyzed as previously described (Potapenko et al., 2011). Briefly, mIPSCs were recorded as outward currents in ACSF containing tetrodotoxin (TTX, 1 μM), while holding the membrane at −55 mV. mIPSCs were detected using Mini Analysis software (Synaptosoft). The detection threshold was set at 20 pA. Individual PSCs were aligned at the 50% crossing of the rising phase before averaging. PSC frequency and waveform parameters were analyzed using the same software. Charge transfer was calculated by integrating the area under the PSC waveform. mIPSCs were analyzed in periods 2 min before and after focal activation of NMDARs.

NMDA-mediated currents were evoked by focal delivery of NMDA via a second pipette connected to the picospritzer device, or via bath application. Activation of NMDARs by endogenous glutamate levels was assessed following blockade of GLT1 glutamate transporter function. This procedure evoked a persistent, NMDA-mediated tonic current (Fleming et al., 2011), which was quantified by measuring changes in holding current ($I_{holding}$) following bath application of the GLT1 blocker dihydrokainic acid (DHK). 6,7-Dinitroquinoxaline-2,3-dione (DNQX) and DHK were purchased from Ascent Scientific. D-(-)-2-Amino-5-phosphonopentanoic acid (D-AP5), gabazine, ATPγS, and *N*-(2-aminoethyl)-5-isoquinolinesulfonamide dihydrochloride (H-9), were purchased from Tocris Bioscience. NMDA and okadaic acid (OKA) were purchased from Sigma-Adrich.

Statistical analysis. All values are expressed as means ± SEM. Student's paired *t* test was used to compare the effects of a drug treatment on I_{GABAA}. Between group differences (e.g., sham vs HF) were compared using unpaired *t* tests or ANOVA, as indicated, followed by Bonferroni *post hoc* tests. Differences were considered statistically significant at $p < 0.05$ and *n* refers to the number of cells. All statistical analyses were conducted using GraphPad Prism (GraphPad Software).

Results

Sham and HF rats were echocardiographically assessed as previously described (Potapenko et al., 2011), and mean cardiac function values obtained are summarized in Table 1. Compared with sham rats, ligated rats showed a significant increased left ventricle internal dimension throughout the cardiac cycle, a decreased percentage of

Table 1. Summary data of echocardiography measurements of left ventricular parameters obtained from sham ($n = 39$) and HF ($n = 38$) rats

	EF (%)	FS (%)	LVIDd (mm)	LVIDs (mm)
Sham	83.3 ± 5.5	54.7 ± 6.7	8.4 ± 0.6	3.8 ± 0.8
HF	33.9 ± 9.4*	19.1 ± 6.7*	11.0 ± 0.8*	9.0 ± 0.9*

EF, ejection fraction; FS, fractional shortening; LVIDd, left ventricle internal dimension during diastole; LVIDs, left ventricle internal dimension during systole.

*$p < 0.0001$ versus sham.

ejection fraction, and a decreased percentage fractional shortening ($p < 0.0001$ in all cases). Patch-clamp electrophysiological recordings were obtained from a total of 169 SON magnocellular neurosecretory cells (MNCs) obtained from sham rats ($n = 117$ from 39 rats) and HF rats ($n = 52$ from 38 rats).

NMDAR activation potentiates muscimol-evoked GABA$_A$ currents

To measure postsynaptic GABA$_A$-mediated currents (I_{GABAA}) in MNCs, 100 μM muscimol was focally applied to the recorded cells (5–7 psi, 0.1 s). As shown in Figure 1 and at a holding potential of −55 mV, muscimol evoked a large outward current (I_{GABAA}), which was completely blocked by the GABA$_A$R blocker gabazine (15 μM).

To determine whether activation of NMDARs modulated the magnitude of I_{GABAA}, muscimol was focally applied before and during bath application of 30 μM NMDA (Fig. 1*B*). As expected, bath-applied NMDA induced a slowly developing, noninactivating inward current (peak $I_{NMDA} = 360.0 \pm 40.6$ pA), which was completely blocked by the NMDAR blocker D-AP5 (100 μM, data not shown). Remarkably, I_{GABAA} evoked during the plateau phase of I_{NMDA} displayed a significantly larger charge transfer (~90% increase, $p < 0.02$, $n = 10$), compared with that evoked in control ACSF. A plot of ΔI_{GABAA} as a function of I_{NMDA} peak failed to reveal a significant correlation between these two parameters ($R^2 = 0.1$, Fig. 1*D*).

In a subset of experiments, we also obtained recordings from presympathetic neurons in the PVN that innervate the rostral ventrolateral medulla (PVN-RVLM). As shown in Figure 2, bath application of 30 μM NMDA induced an inward current (peak I_{NMDA}, 571.3 ± 63.8 pA) and also significantly increased I_{GABAA} charge transfer in this neuronal population (~170%, $p < 0.05$, $n = 6$). The remainder of the study, however, was focused on MNCs.

To better study the time course and duration of the NMDA-evoked potentiation of I_{GABAA}, muscimol was repetitively applied (90 s intervals) before and after a single brief, focal application of NMDA (30 μM, 15 s). Results are summarized in Figure 3. Focal NMDA application resulted in an inward current of 698.9 ± 238.4 pA, with a clear transient and sustained components. This focal and briefer NMDA stimulus was still able to evoke a significant increase in I_{GABAA} charge transfer (118.2 ± 25.1% change at peak, $n = 12$, $p < 0.01$). Interestingly, however, we identified two distinct patterns in the time course of the I_{GABAA} potentiation by NMDA. In a subset of neurons ($n = 5$), a rapid and transient potentiation of I_{GABAA} was observed ($p < 0.01$, one-way repeated-measures ANOVA), with a peak occurring in the first muscimol application following NMDAR activation (i.e., 90 s), and a full recovery back to baseline at 270 s (Fig. 3*B*). Conversely, a slower, longer-lasting effect was observed in the remaining neurons ($n = 6$) ($p < 0.001$, one-way repeated-measures ANOVA), which showed a peak potentiation of I_{GABAA} at 460 s following NMDAR activation. I_{GABAA} magnitude started to diminish thereafter, with a partial recovery of ~50% at 810 s (Fig. 3*B*). While in some cases the recording conditions deteriorated during these protocols, in three of six cells we were able to observe a full recovery of I_{GABAA} back to control levels between 1260 and 1530 s after NMDAR stimulation.

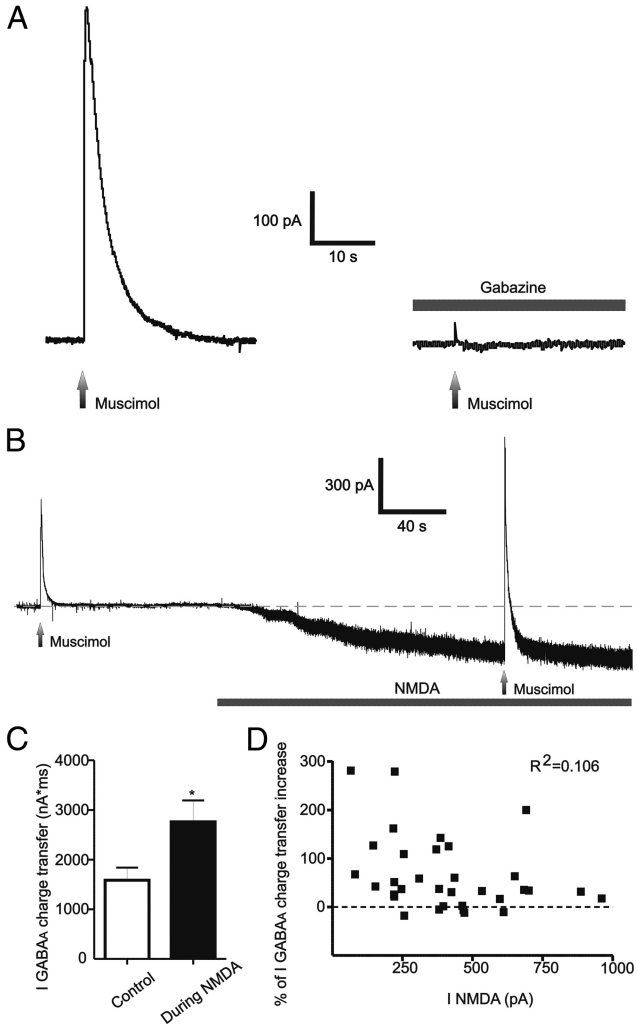

Figure 1. NMDAR activation enhanced I_{GABAA} magnitude in MNCs. ***A***, Representative example of an outward current evoked by a puff of muscimol (100 μM, 0.1 s, 5 psi), which was blocked by the GABA$_A$R antagonist gabazine (15 μM). ***B***, Representative example of a muscimol-evoked I_{GABAA} before and during bath application of 30 μM NMDA. Note the enhanced magnitude of I_{GABAA} during NMDAR activation. ***C***, Summary data showing mean I_{GABAA} magnitude before and during NMDA application ($n = 10$). ***D***, Plot of I_{GABAA} magnitude as a function of the NMDA-mediated current (I_{NMDA}), showing lack of correlation between both parameters. *$p < 0.05$. All recordings were obtained from sham rats.

The peak potentiation of I_{GABAA} was significantly larger in the group of neurons showing a slower time course, when compared with those showing a faster time course (162.8 ± 31.7% vs 55.7 ± 19.8%, respectively, $p < 0.05$). The difference in the time course, or overall magnitude of the I_{GABAA} potentiation, was not due to differences in I_{NMDA} magnitude (623.3 ± 128.7 pA vs 724.0 ± 83.6 pA, $p > 0.5$), or to differences in the basal magnitude of I_{GABAA} (84.7 ± 28.0 nA*ms vs 81.5 ± 19.9 nA*ms, $p > 0.9$). Moreover, recordings obtained from transgenic eGFP-VP rats showed that both eGFP-VP and non-eGFP-VP neurons were observed in both groups (2 eGFP-VP and 2 non-eGFP-VP neurons displayed a slow pattern, whereas 1 eGFP-VP and 1 non-eGFP-VP neurons displayed a fast potentiation pattern). Thus, differences in the time course of NMDA-mediated potentiation of I_{GABAA} appear to be cell-type independent. focal NMDA appli-

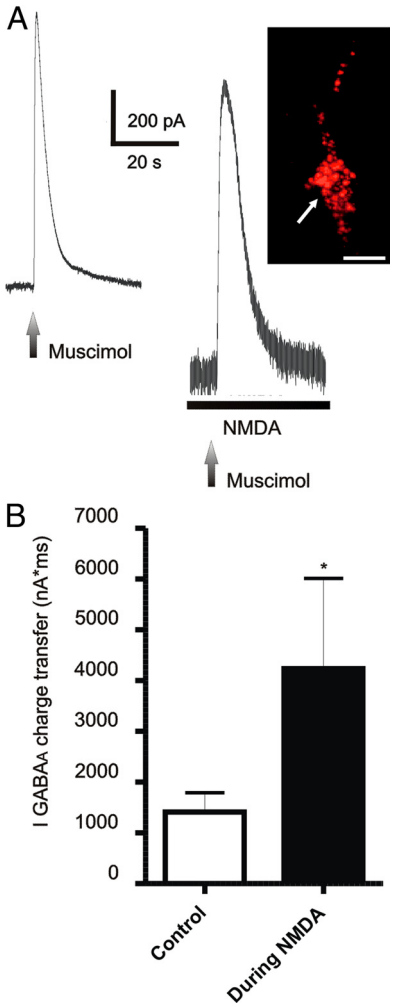

Figure 2. NMDAR activation enhanced I_{GABAA} magnitude in presympathetic PVN-RVLM projecting neurons. ***A***, Representative example of a muscimol-evoked I_{GABAA} before and during bath application of 30 μM NMDA in a PVN-RVLM neuron. Note the enhanced magnitude of I_{GABAA} during NMDAR activation. Inset, Photomicrograph of the recorded PVN-RVLM neuron (arrow) showing retrograde labeling with rhodamine beads. ***B***, Summary data showing mean I_{GABAA} magnitude before and during NMDA application ($n = 6$). Scale bar, 15 μm. *$p < 0.05$. All recordings were obtained from sham rats.

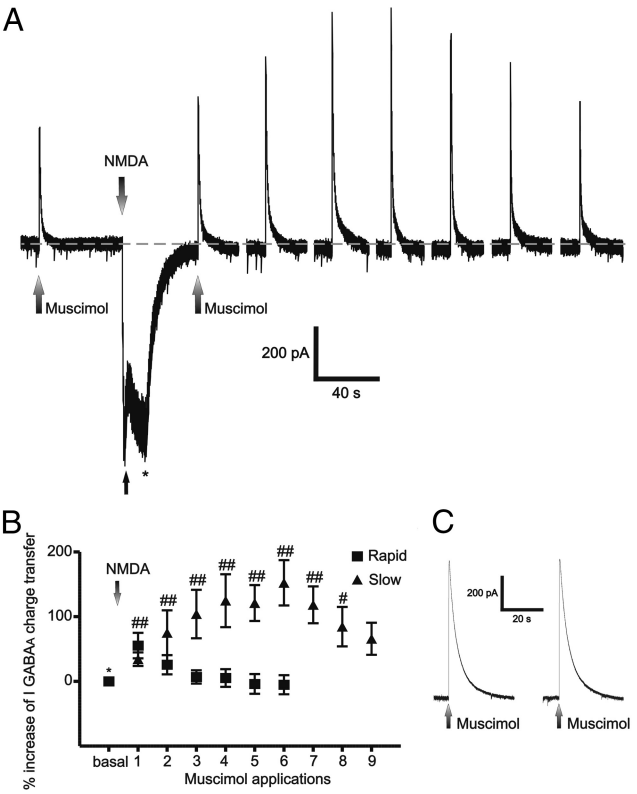

Figure 3. Time course of NMDA-mediated I_{GABAA} potentiation. ***A***, Representative example showing repetitive muscimol-evoked I_{GABAA} (90 s interval) before and after focal application of NMDA (30 μM, 15 s). Note the transient (arrow) and sustained (asterisk) components of the evoked NMDA current. ***B***, Summary data showing mean percentage changes in I_{GABAA} during repetitive applications of muscimol following a focal NMDA application. Two response patterns were observed, including neurons showing a slow onset and slow recovery (triangles, $n = 6$) and neurons showing a fast onset, fast recovery response (squares, $n = 5$). *$p < 0.01$ versus basal (fast); $^{\#}p < 0.05$ and $^{\#\#}p < 0.01$ versus basal (slow), Dunnett's multiple-comparison *post hoc* test. ***C***, Representative example of two repetitive muscimol-evoked I_{GABAA} (90 s interval) in control conditions, showing lack of differences between the first and second applications. All recordings were obtained from sham rats.

cation for 5 s ($n = 4$) failed to potentiate I_{GABAA} currents ($p > 0.5$, data not shown). As shown in Fig. 3*C*, the magnitude of I_{GABAA} did not change when two consecutive applications of muscimol were performed in the absence of NMDAR stimulation (first muscimol: 738.3 ± 143.4 nA*ms; second muscimol: 716.9 ± 138.8 nA*ms, $p > 0.1$, $n = 5$, 90 s interval).

NMDAR activation potentiates muscimol and synaptically mediated GABA$_A$ currents in a nitric oxide-independent manner

It was previously shown that activation of NMDARs in MNCs stimulate presynaptic GABA release via the retrograde signaling molecule nitric oxide (NO) (Bains and Ferguson, 1997). In fact, in some cases, as shown in the representative example of Fig. 4*A*, an increase in the frequency of GABA$_A$ IPSCs during NMDAR activation was also observed in our study. Thus, we wanted to determine whether the NMDA-mediated potentiation of muscimol-evoked I_{GABAA} was dependent or not on NO production. Moreover, we also assessed whether synaptically mediated GABA$_A$ currents were also enhanced following NMDAR activation. Slices were preincubated with the NO synthase blocker *N*-nitro-L-arginine methyl ester (L-NAME) (1 mM). As shown in Fig. 4*B,C*, muscimol-evoked I_{GABAA} charge transfer was still enhanced following NMDAR activation in the presence of L-NAME ($p < 0.05$, $n = 4$). In line with previous studies (Bains and Ferguson, 1997; Nicholson et al., 2004), we found the I_{NMDA} magnitude in the presence of L-NAME to be significantly larger than that in control conditions (peak I_{NMDA}, 819.8 ± 75.6 pA, $p < 0.0001$).

To determine whether synaptic GABA$_A$Rs were also potentiated following NMDAR activation, we recorded miniature GABA$_A$ IPSCs (mIPSCs) in the presence of TTX and L-NAME. For these studies, we used a brief focal application of NMDA to avoid potential problems in IPSC detection due to the large increase in baseline noise during prolonged NMDA bath application. As shown in Fig. 4*D–G*, the mIPSC charge transfer was significantly enhanced following NMDAR activation ($p < 0.05$, paired-*t* test, $n = 6$). Conversely, mIPSC frequency was not changed following NMDAR activation ($p > 0.5$, $n = 6$, data not shown).

Activation of extrasynaptic NMDARs following blockade of astrocyte GLT1 glutamate transporter potentiates evoked GABA$_A$ currents

We recently demonstrated the presence of functional extrasynaptic NMDARs (eNMDARs) in MNCs, which are activated by

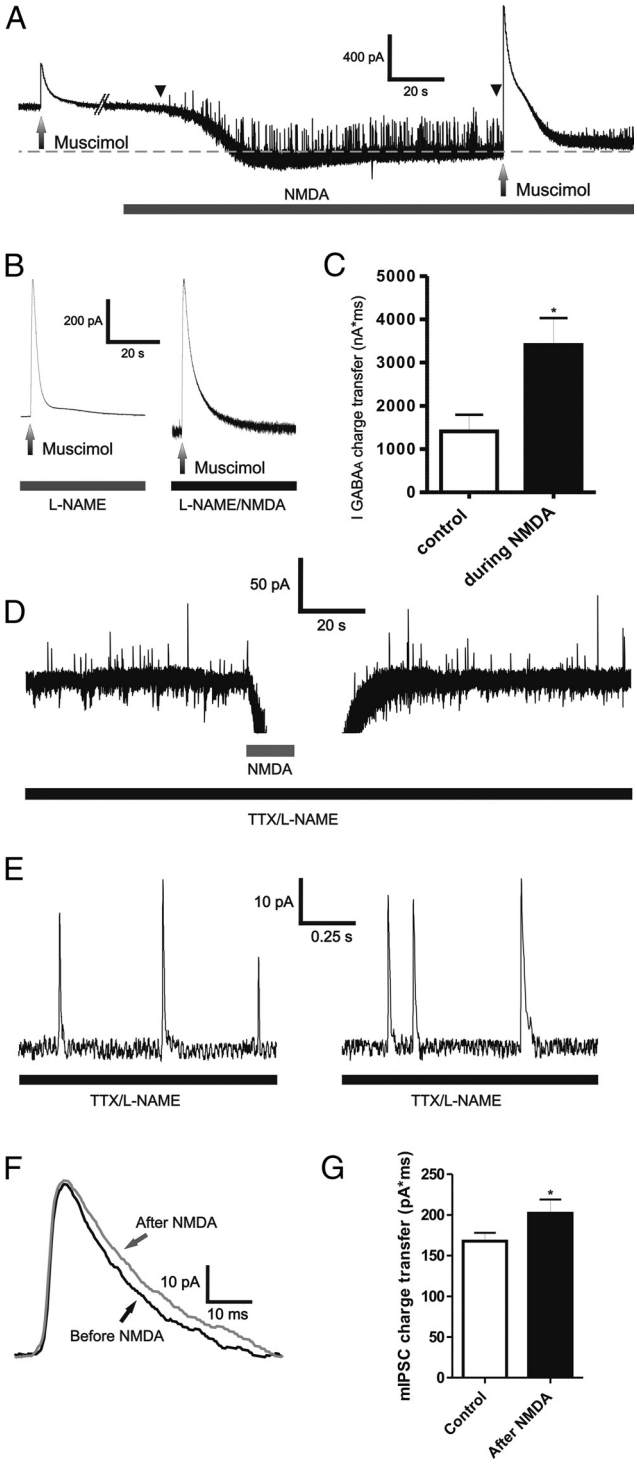

Figure 4. NMDAR activation enhanced muscimol and synaptically mediated I_{GABAA} in a NO-independent manner. ***A***, Representative example depicting an increased in the frequency of outward IPSCs (between arrowheads) during bath application of 30 μM NMDA. ***B***, Representative example of a muscimol-evoked I_{GABAA} before and during bath application of 30 μM NMDA in the presence of the NO synthase blocker L-NAME (1 mM). ***C***, Summary data showing the mean I_{GABAA} magnitude before and during NMDA application in the presence of L-NAME ($n = 4$). ***D***, Representative example depicting outward mIPSCs (arrows), before and after focal application of NMDA (30 μM, 5 s). Lower traces show segments of mIPSC for each period, at a more expanded time scale. ***E***, The averaged mIPSC corresponding to the periods before and after NMDA application for the MNC shown in ***D*** are depicted. ***F***, Representative example of the averaged mIPSC before and after NMDA application. ***G***, Summary data showing mean mIPSC charge transfer before and after NMDA puff in the presence of TTX and L-NAME ($n = 6$). *$p < 0.05$ versus respective controls. All recordings were obtained from sham rats.

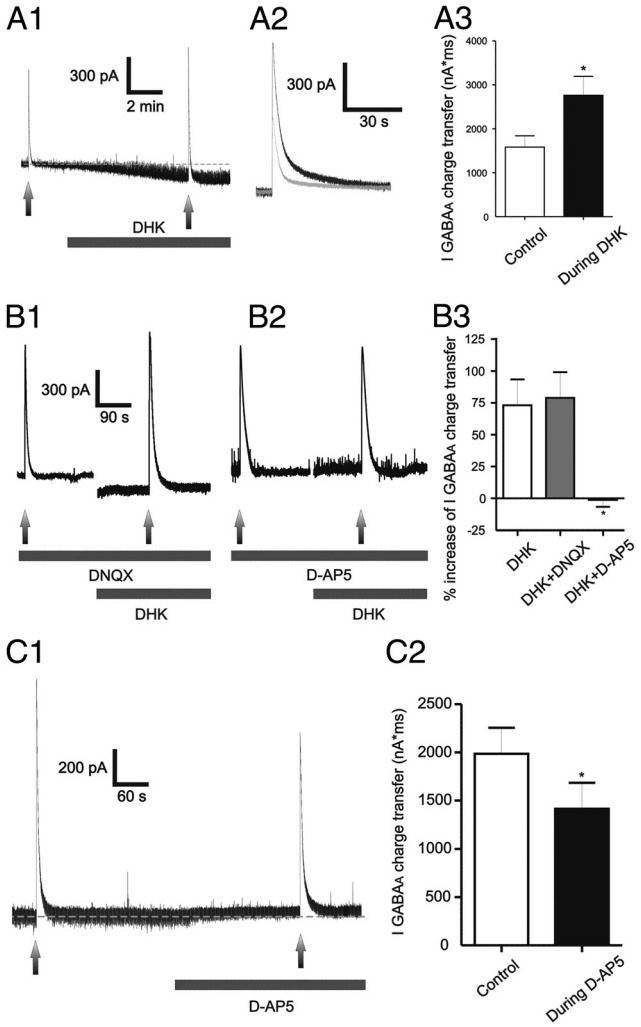

Figure 5. Blockade of astrocyte glutamate transporter GLT1 induced an NMDA-mediated tonic inward current (tonic I_{NMDA}) that potentiated I_{GABAA}. ***A1–A3***, Representative example of a muscimol-evoked I_{GABAA} before and during bath application of DHK (500 μM). Note the inward shift in $I_{holding}$ (tonic I_{NMDA}) during DHK application, and the enhanced I_{GABAA} magnitude in the presence of DHK (***A1***). ***A2***, Segments of traces showing I_{GABAA} before (gray) and during (black) DHK application were superimposed for better comparisons. The mean I_{GABAA} magnitude before and during DHK application is shown in ***A3*** ($n = 8$). ***B1–B3***, Representative traces showing that the potentiation of I_{GABAA} during DHK application persisted when AMPARs were blocked (DNQX, 10 μM, ***B1***), but was blocked when NMDARs were blocked (D-AP5 100 μM, ***B2***). The summary data are shown in ***B3*** ($n = 8$, 4, and 6 for DHK, DHK plus DNQX, and DHK plus D-AP5, respectively). ***C1***, ***C2***, Representative trace showing that blockade of basal tonic I_{NMDA} (D-AP5, 100 μM) reduced the magnitude of I_{GABAA} (***C1***). Note the outward shift in $I_{holding}$ evoked by D-AP5. The summary data ($n = 8$) is shown in ***C2***. *$p < 0.05$ versus control (***A3*** and ***C2***), or DHK (***B3***). All recordings were obtained from sham rats.

extracellular ambient glutamate, whose levels are tightly controlled by the activity of GLT1 astrocyte glutamate transporters (Fleming et al., 2011). Thus, to determine whether activation of eNMDARs under astrocyte control also enhanced the efficacy of I_{GABAA}, muscimol was focally applied before and during astrocyte GLT1 blockade with bath-applied DHK (500 μM). As previously reported (Fleming et al., 2011), DHK induced a slowly developing, noninactivating inward current (79.8 ± 12.2 pA, $n = 8$) (Fig. 5*A*). Similar to NMDA, I_{GABAA} charge transfer was robustly enhanced in the presence of DHK (~100%, $p < 0.05$, Fig. 5*A*).

In agreement with our previous results showing that the DHK-evoked current was mediated by activation of NMDARs,

but not AMPARs (Potapenko et al., 2012), we found that the DHK-evoked potentiation of I_{GABAA} was still observed in the presence of the AMPAR blocker DNQX (10 μM), but was completely blocked by the NMDAR blocker D-AP5 (100 μM) (Fig. 5*B*).

eNMDARs in MNCs are tonically activated by endogenous glutamate levels, resulting in a tonic, persistent NMDA inward current (tonic I_{NMDA}) (Fleming et al., 2011; Potapenko et al., 2012). Thus, we addressed whether persistent activation of eNMDARs tonically influenced GABA$_A$R strength. To this end, we focally applied muscimol before and after blocking tonic I_{NMDA} with bath-applied AP5. As previously reported (Fleming et al., 2011; Potapenko et al., 2012), bath application of AP5 (100 μM) induced an outward shift in $I_{holding}$ and reduced baseline root mean square (rms) noise ($\Delta I_{holding}$: 16.2 ± 4.9 pA; Δ rms: 2.9 ± 0.7 pA, respectively, $n = 8$, $p < 0.02$ in both cases, paired *t* test). As shown in Fig. 5*C*, blockade of basal tonic I_{NMDA} diminished I_{GABAA} magnitude (30.6 ± 7.7%, $n = 8$, $p < 0.05$, paired *t* test).

Given similar results obtained following activation of NMDARs by endogenous glutamate (i.e., following GLT1 blockade) or by exogenously applied NMDA, subsequent data were pooled together for further analysis.

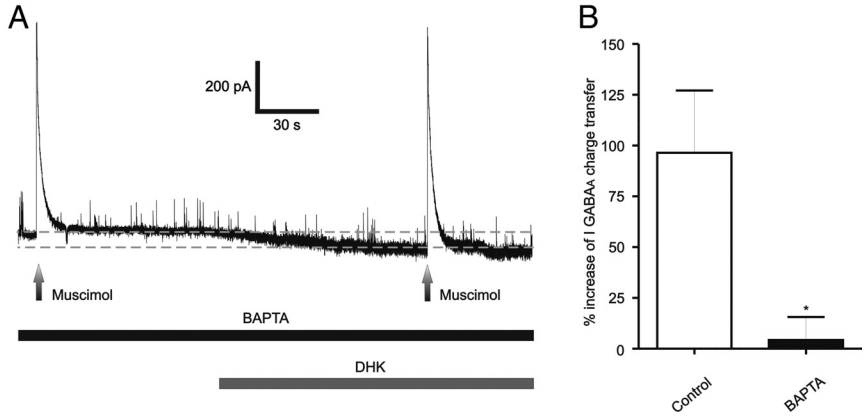

Figure 6. NMDAR–GABA$_A$R coupling is Ca^{2+}-dependent. ***A***, Representative trace showing that the potentiation of I_{GABAA} during DHK application was blocked when recorded neurons were intracellularly dialyzed with the Ca^{2+} chelator BAPTA (10 μM). ***B***, Summary data showing percentage changes in I_{GABAA} magnitude in control conditions and in cells dialyzed with BAPTA. *$p < 0.02$, $n = 15$. All recordings were obtained from sham rats.

The NMDAR–GABA$_A$R crosstalk is dependent on a rise in intracellular Ca^{2+} levels

To determine whether the NMDAR-mediated potentiation of I_{GABAA} was dependent on a rise of intracellular Ca^{2+}, cells were preloaded with the fast Ca^{2+} chelator BAPTA (10 mM) through the recording patch pipette. A representative example is shown in Figure 6*A*. We found that intracellular BAPTA prevented the effects of NMDAR activation on I_{GABAA} magnitude ($n = 6$ DHK and 9 NMDA), resulting in significant differences when compared with DHK/NMDA-evoked responses in control conditions (Fig. 6*B*). The magnitude of the NMDA-evoked currents, on the other hand, was not affected by BAPTA (DHK-BAPTA: 98.3 ± 53.3 pA, $p > 0.6$ vs DHK non-BAPTA; NMDA-BAPTA: 465.6 ± 48.9 pA, $p > 0.1$ vs NMDA non-BAPTA), indicating that the blunted potentiation of I_{GABAA} by BAPTA was not due to changes in the NMDA-evoked currents.

The NMDAR–GABA$_A$R crosstalk is dependent on intracellular kinase activity

Previous studies have shown that NMDAR activation can lead to Ca^{2+}-dependent changes in the intracellular kinase–phosphatase balance (Colbran, 2004), which in turn can affect GABA$_A$R properties (Morishita and Sastry, 1996; Wang and Stelzer, 1996; Gaiarsa et al., 2002; Kawaguchi and Hirano, 2002). To test whether NMDAR-mediated potentiation of I_{GABAA} was dependent on the intracellular kinase–phosphatase balance, we pharmacologically shifted this balance toward either a phosphatase predominance (using the broad-spectrum kinase blocker H-9 hydrochloride) or toward a kinase predominance, using the PP1/PP2a phosphatase blocker OKA (Ishihara et al., 1989), or ATPγS, a nonhydrolysable analog of ATP. Results are summarized in Figure 7. NMDAR-mediated potentiation of I_{GABAA} persisted following intracellular blockade of PP1/PP2a phosphatase activity [OKA 1 μM, ~70% increase, $p < 0.02$, $n = 15$ (8 DHK and 7 NMDA)]. On the other hand, the NMDA-mediated potentiation was significantly diminished in MNCs dialyzed with 50 μM H-9, resulting in a proportionally smaller effect than that observed in control conditions [~30%, $n = 14$ (7 DHK and 7 NMDA), $p < 0.05$ vs control, Fig. 7*B*,*C*]. Finally, the NMDAR-mediated potentiation of I_{GABAA} was even further blocked by intracellular dialysis with ATPγS (100 μM), $p > 0.4$, $n = 9$ (6 DHK and 3 NMDA). Interestingly, when compared with control conditions, the basal I_{GABAA} magnitude was significantly increased by ATPγS ($p < 0.05$), but not by OKA or H-9 (Fig. 7*B*).

Blunted eNMDAR–GABA$_A$R crosstalk in HF rats

To determine whether the NMDAR–GABA$_A$R coupling was altered in HF rats, similar experiments with DHK were performed in this experimental group ($n = 52$ MNCs from HF rats). As shown in Figure 8*A*, activation of NMDARs either following GLT1 blockade with bath-applied DHK (500 μM, $n = 7$) or NMDA ($n = 6$) failed to significantly enhance I_{GABAA} magnitude ($p > 0.1$). Given possible differences in cell size between sham and HF conditions, results were expressed as current density (see Materials and Methods). As shown in Figure 8*B*, NMDAR activation significantly enhanced I_{GABAA} current density in sham, but not in HF rats ($p < 0.01$ and $p > 0.1$, respectively, Bonferroni *post hoc* tests). The basal magnitude of I_{GABAA} current density was not significantly different between MNCs from sham or HF rats ($p > 0.05$, Bonferroni *post hoc* test). Importantly, and as recently reported (Potapenko et al., 2012), the magnitude of the DHK-evoked NMDA current was significantly smaller in HF when compared with sham rats (36.9 ± 6.3 pA, $p < 0.05$ vs sham rats; see above). However, we found no significant correlation between the DHK-evoked current magnitude and the degree of I_{GABAA} modulation when data from both sham and HF rats were combined (R^2, 0.006). On the other hand, I_{NMDA} evoked by direct activation with the agonist NMDA in HF rats (386.0 ± 30.5 pA) was similar to that evoked in sham rats ($p > 0.6$). Together, these data suggest that the differences in I_{GABAA} modulation observed between sham and HF rats were not due to a diminished degree of NMDAR activation.

Despite the blunted NMDAR–GABA$_A$R crosstalk in HF rats, we tested the effects of phosphatase and kinase blockade in MNCs from these rats. Results are summarized in Figure 8*C*. As shown,

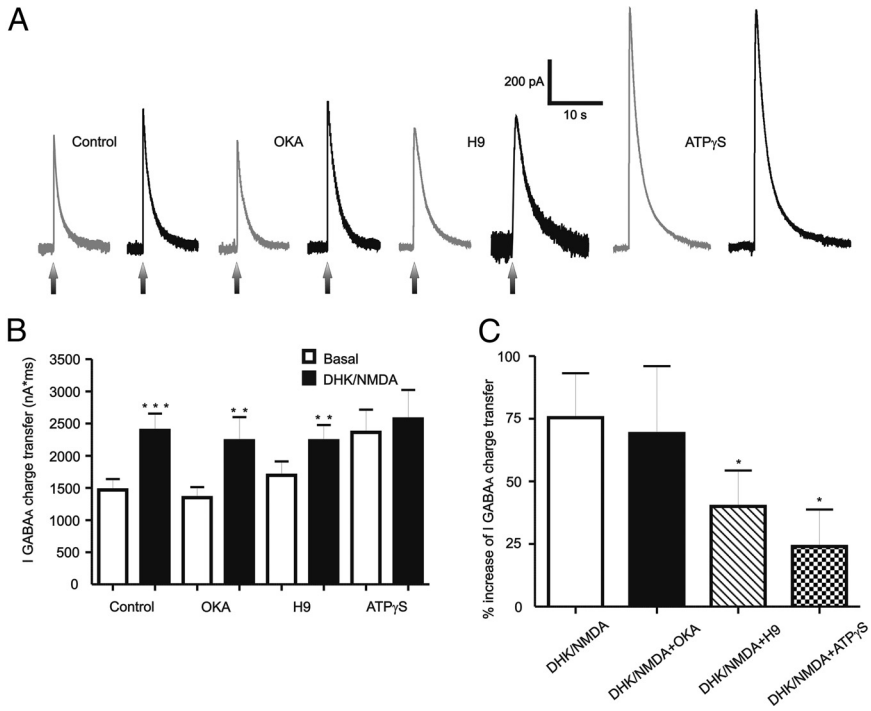

Figure 7. Kinase activity is required for the NMDA-mediated potentiation of I_{GABAA}. ***A***, Representative traces showing the effects of NMDA (30 μM) on I_{GABAA} in MNCs intracellularly dialyzed with the PP1/PP2a phosphate blocker OKA (1 μM), or the broad-spectrum kinase blocker H-9 (50 μM), or with ATPγS (100 μM). ***B***, Summary data showing mean I_{GABAA} magnitude in control conditions, and in MNCs dialyzed with OKA, H-9, or ATPγS ($n = 17, 15, 14$, and 9, respectively). ***C***, Summary data showing mean percentage change in I_{GABAA} induced by NMDA in the same recording conditions as in ***B***. *$p < 0.05$ versus control (***C***); **$p < 0.02$ and ***$p < 0.001$ versus respective basal (***B***). All recordings were obtained from sham rats.

NMDAR activation still failed to significantly stimulate I_{GABAA} in HF rats in all conditions tested ($p > 0.1$ in all cases).

Discussion

We describe here a novel form of glutamate–GABA interactions that involve crosstalk between NMDA and GABA$_A$ postsynaptic receptors in MNCs. We show that (1) activation of NMDARs, either by an exogenous agonist or by endogenous glutamate controlled by glial GLT1 glutamate transporters, potentiated muscimol-evoked GABA$_A$R-mediated current (I_{GABAA}), as well as GABA$_A$ mIPSCs; (2) the NMDAR–GABA$_A$R crosstalk was prevented by chelation of intracellular Ca^{2+} or by intracellular kinase activity blockade; (3) the NMDAR–GABA$_A$R crosstalk was blunted in MNCs from rats with HF, a disease in which MNCs are overly activated, contributing in turn to neurohumoral activation, a hallmark of this disease (Cohn et al., 1981); and (4) the NMDAR–GABA$_A$R crosstalk was also observed in presympathetic PVN-RVLM projecting neurons, which contribute to the physiological control of sympathetic outflow and to sympathoexcitation in HF (Yang and Coote, 1998; Patel, 2000; Han et al., 2010).

NMDAR activation potentiates GABA$_A$ currents

Our results show that NMDARs in MNCs mediate a short-term form of GABA$_A$R-mediated inhibitory plasticity involving interreceptor crosstalk at a postsynaptic locus. Both synaptic (i.e., mIPSCs) and nonsynaptic (muscimol) GABA$_A$-mediated currents were potentiated following NMDAR activation. Proportionally, muscimol-evoked I_{GABAA} was more prominently potentiated than mIPSCs. Whether this was due to a differential sensitivity between synaptic and nonsynaptic GABA$_A$Rs to NMDAR-mediated effects, or simply due to the fact that a substantially larger number of GABA$_A$Rs are engaged following muscimol application, is at present unknown.

We observed two types of temporal patterns in the NMDA-evoked GABA$_A$R potentiation. One was characterized by a relatively rapid onset and recovery time course, with an I_{GABAA} potentiation of ~50%. The other was characterized by a slower onset and recovery time course, and a larger I_{GABAA} potentiation (~160%). These differential patterns were independent of the cell type (i.e., vasopressin vs oxytocin) or the magnitude of I_{NMDA} or basal I_{GABAA}. Given our results showing the NMDAR–GABA$_A$R crosstalk to be Ca^{2+}-dependent, it is possible that these distinct time courses could result from cell–cell variability in the waveform of the NMDA-evoked $\Delta[Ca^{2+}]_i$.

The enhancement of GABA$_A$R function was observed following at least 5–15 s of persistent NMDAR stimulation, with either bath or focally delivered NMDA. These approaches likely activated both synaptic NMDARs and eNMDARs, two molecularly and functionally distinct pools of NMDARs (Hardingham and Bading, 2010). While synaptic NMDARs display a high affinity for glutamate, they rapidly desensitize following sustained activation. Conversely, eNMDARs display much lower affinity, but do not desensitize in the presence of sustained levels of glutamate. Therefore, eNMDARs are better suited to be activated by spillover of glutamate during synchronous activation of afferent inputs, or by low extracellular glutamate levels (Le Meur et al., 2007; Fleming et al., 2011). Given this, our studies support the participation of eNMDARs in the reported NMDAR–GABA$_A$R coupling. We recently showed that eNMDARs in MNCs are tonically activated by extracellular glutamate, whose levels are tightly controlled by astrocyte GLT1 glutamate transporters. We found that GLT1 blockade resulted in a buildup of extracellular glutamate and activation of eNMDARs, leading to a persistent tonic current (tonic I_{NMDA}) and a concomitant increase in MNC firing discharge (Fleming et al., 2011). Our present results, showing that blockade of GLT1 activity potentiated GABA$_A$R function via activation of NMDARs, further support a contribution of eNMDARs to GABA$_A$R potentiation. Moreover, these studies underscore the pivotal role that astrocytes play in regulating the NMDAR–GABA$_A$R coupling efficacy.

Importantly, we found that blockade of basal tonic I_{NMDA} diminished the magnitude of the evoked I_{GABAA}, suggesting that the persistent activation of a small proportion of eNMDARs by ambient glutamate is sufficient to continuously stimulate GABA$_A$R function. Therefore, our findings support a dual action of eNMDARs on GABA inhibitory function. First, their persistent activation by low ambient glutamate levels may contribute to setting a basal degree of GABA$_A$R strength. Second, suprabasal activation of eNMDARs, either by diminished glial glutamate transporter activity, or by glutamate spillover dur-

ing robust afferent synaptic activity, would lead to a prominent GABA$_A$R potentiation, acting in turn as a compensatory, counterbalancing mechanism to dampen overexcitation.

The NMDAR–GABA$_A$R coupling is Ca^{2+}-dependent and kinase-dependent

The NMDA-mediated potentiation of I_{GABAA} was blocked by intracellular BAPTA, indicating that the inter-receptor coupling was dependent on a rise of $[Ca^{2+}]_i$. One mechanism by which an NMDA-mediated $\Delta[Ca^{2+}]_i$ could affect GABA$_A$R function is via Ca^{2+}-dependent production of NO, previously shown to presynaptically increase GABA release (Bains and Ferguson, 1997; Stern and Ludwig, 2001). However, our results, showing that the postsynaptic NMDAR–GABA$_A$R coupling persisted when NO synthase activity was blocked, would argue against this mechanism. Alternatively, a $\Delta[Ca^{2+}]_i$ could influence GABA$_A$R function by altering the intracellular phosphate–kinase balance (Krishek et al., 1994; Jones and Westbrook, 1997; Poisbeau et al., 1999). Previous studies showed that neurosteroid-mediated enhancement of GABA$_A$ IPSC magnitude in MNCs was dependent on PKC activation (Fáncsik et al., 2000; Brussaard and Koksma, 2002). Here, we found that broad-spectrum blockade of kinase (but not PPD1/2 phosphatase) activity prevented the NMDA-mediated potentiation of I_{GABAA}, suggesting that the NMDAR–GABA$_A$R coupling is mediated by a Ca^{2+}/kinase-dependent phosphorylation mechanism. This is further supported by our results showing that ATPγS, a nonhydrolysable analog of ATP (Eckstein, 1985) per se, potentiated I_{GABAA}, occluding the subsequent effect of NMDA. While the most parsimonious interpretation is that NMDAR activation resulted in direct GABA$_A$R phosphorylation, other alternatives should be considered, including Ca^{2+}-dependent and phosphorylation-dependent increase of GABA$_A$R trafficking to the membrane surface (Marsden et al., 2007).

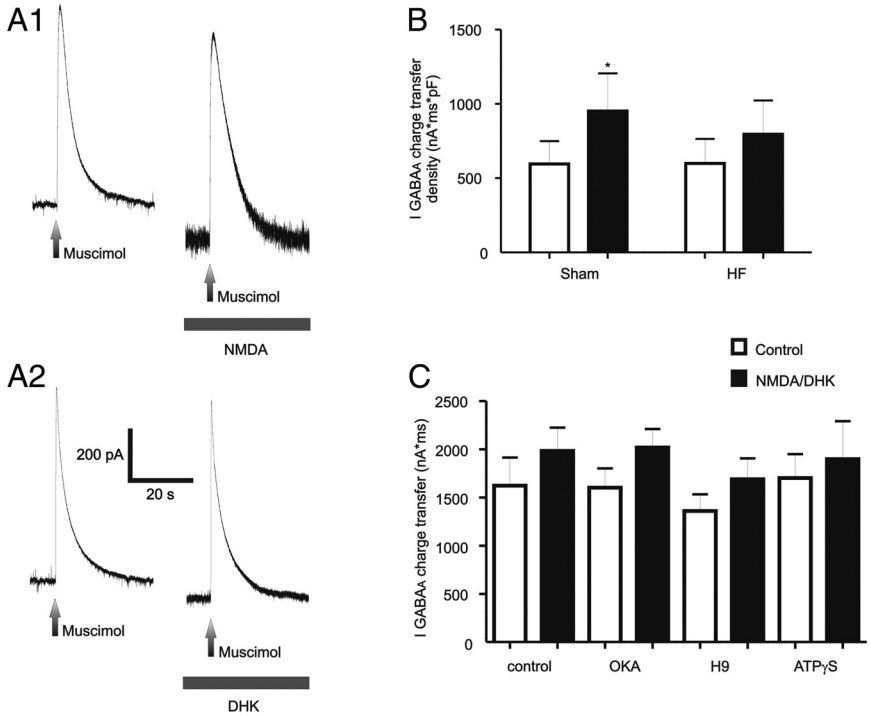

Figure 8. NMDAR–GABA$_A$R crosstalk is blunted in rats with HF. ***A1, A2***, Representative traces showing lack of I_{GABAA} potentiation following activation of NMDARs either with NMDA (30 μM, ***A1***), or by endogenous glutamate following GLT1 blockade with DHK (500 μM, ***A2***). ***B***, Summary data showing mean I_{GABAA} charge transfer density before and after NMDAR activation in sham and HF rats ($n = 18$ and 13, respectively). ***C***, Summary data showing lack of effects of intracellular dialysis with OKA, H-9, or ATPγS on the blunted NMDA-mediated I_{GABAA} potentiation in MNCs from HF rats ($n = 13$, 20, 13, and 6, respectively). *$p < 0.01$ versus control.

Functional implications of NMDAR–GABA$_A$R coupling in physiological and pathological conditions

Glutamate and GABA, acting primarily on NMDARs and GABA$_A$Rs, respectively, are the main excitatory and inhibitory neurotransmitters influencing MNC activity (Randle and Renaud, 1987; Decavel and Van den Pol, 1990; van den Pol et al., 1990; Hu and Bourque, 1992; Nissen et al., 1995; Bains and Ferguson, 1997). The characteristics of the NMDAR–GABA$_A$R coupling reported here would imply that during a time window following NMDAR activation, gating of GABA$_A$Rs, by either incoming GABAergic inputs, or by extracellular ambient GABA levels (Park et al., 2006), would result in a more robust inhibitory action, effectively dampening NMDA-mediated excitation. Thus, the NMDA–GABA$_A$ inter-receptor crosstalk may serve as a counterbalancing, inhibitory feedback mechanism. This is in line with a previous study in MNCs showing that blockade of NMDA-NO-mediated increase in GABA IPSCs frequency (following NO synthase blockade) potentiated the NMDA excitatory effect (Bains and Ferguson, 1997). Since we observed similar NMDAR–GABA$_A$R crosstalk in PVN-RVLM neurons, it is reasonable to speculate that a similar mechanism will influence PVN regulation of sympathoexcitatory outflow. Indeed, previous *in vivo* studies showed that GABA$_A$R blockade within the PVN evoked sympathoexcitatory responses that were largely blunted by previous NMDAR blockade in this nucleus (Chen et al., 2003; Li et al., 2006), implying that NMDAR activation tonically supports a GABA$_A$R-mediated tonic inhibition within the PVN.

Together, these studies support the notion that NMDARs potentiate GABA function through at least two complementary mechanisms, a presynaptic NO-dependent mechanism and a postsynaptic NO-independent mechanism, which, acting in parallel, serve as a potent feedback inhibitory system to restrain overexcitation following NMDAR activation (Fig. 9, model).

It is reasonable to speculate, on the other hand, that a diminished efficacy of this counterbalancing mechanism would result in an enhanced NMDA-mediated excitatory effect in MNCs. Indeed, we found a blunted NMDA-mediated potentiation of I_{GABAA} in MNCs of rats with congestive HF, supporting an uncoupling between these major neurotransmitter receptors. HF is a syndrome characterized by an increased neurohumoral drive, which involves augmented sympathetic tone and elevated hormonal plasma levels, including vasopressin (Packer, 1988), the latter contributing to altered fluid–electrolyte balance and detrimental myocardial effects in HF patients (Goldsmith et al., 1986; Packer et al., 1987). A growing body of evidence supports an enhanced glutamate excitatory action (Li et al., 2003; Kleiber et al., 2008; Kang et al., 2009; Potapenko et al., 2011; Zheng et al., 2011), along with blunted GABAergic inhibitory actions (Zhang et al., 2002; Han et al., 2010;

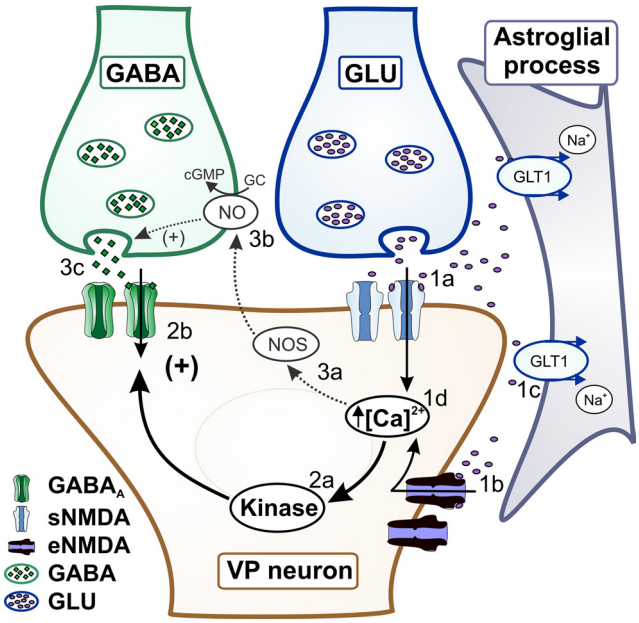

Figure 9. Schematic model showing complementary modalities of NMDAR–GABA$_A$R interactions in MNCs. Activation of sNMDARs by synaptically released glutamate (1a), or activation of eNMDARs by ambient extracellular glutamate levels (1b) controlled by astrocyte GLT1 transporters (1c), results in an increase in $[Ca^{2+}]_i$ (1d). The $\Delta[Ca^{2+}]_i$ leads to activation of kinase activity (2a), resulting in turn in potentiation of postsynaptic GABA$_A$Rs (2b). In parallel, the $\Delta[Ca^{2+}]_i$ stimulates NO synthase activity (3a), resulting in NO production and retrograde diffusion in the synaptic cleft (3b), stimulating in turn presynaptic release of GABA (3c).

Potapenko et al., 2011) involving both neurosecretory and presympathetic hypothalamic neurons in HF rats. Thus, our studies suggest that a blunted NMDAR–GABA$_A$R coupling may constitute an underlying mechanism contributing to the imbalanced excitatory–inhibitory state, and enhanced MNC activation during HF (Patel et al., 1993, 2000; Vahid-Ansari and Leenen, 1998; Han et al., 2010). The NMDAR–GABA$_A$R uncoupling during HF could be due to multiple factors, including blunted NMDA-mediated $\Delta[Ca^{2+}]_i$, altered kinase–phosphatase balance, and/or a switch in GABA$_A$R subunit composition. A blunted NO synthase expression and function in the SON and PVN (Zhang et al., 2001; Biancardi et al., 2011) is known to contribute to blunted GABAergic function and increased neurohumoral drive in HF rats (Zhang et al., 2002; Patel and Zheng, 2012). However, our results showing lack of NO involvement in the NMDA–GABA$_A$ postsynaptic receptor crosstalk, would argue against a role for NO in this case. Thus, a combination of both presynaptic (NO-mediated) and postsynaptic uncoupling between NMDARs and GABA$_A$Rs contribute to enhanced NMDA-mediated excitation and neurohumoral activation in HF. Future studies aiming to identify the specific mechanism underlying the postsynaptic NMDAR–GABA$_A$R uncoupling in HF are warranted.

References

Bains JS, Ferguson AV (1997) Nitric oxide regulates NMDA-driven GABAergic inputs to type I neurones of the rat paraventricular nucleus. J Physiol 499:733–746. Medline

Biancardi VC, Son SJ, Sonner PM, Zheng H, Patel KP, Stern JE (2011) Contribution of central nervous system endothelial nitric oxide synthase to neurohumoral activation in heart failure rats. Hypertension 58:454–463. CrossRef Medline

Brussaard AB, Koksma JJ (2002) Short-term modulation of GABAA receptor function in the adult female rat. Prog Brain Res 139:31–42. CrossRef Medline

Cazalis M, Dayanithi G, Nordmann JJ (1985) The role of patterned burst and interburst interval on the excitation-coupling mechanism in the isolated rat neural lobe. J Physiol 369:45–60. Medline

Chen QH, Haywood JR, Toney GM (2003) Sympathoexcitation by PVN-injected bicuculline requires activation of excitatory amino acid receptors. Hypertension 42:725–731. CrossRef Medline

Cohn JN, Levine TB, Francis GS, Goldsmith S (1981) Neurohumoral control mechanisms in congestive heart failure. Am Heart J 102:509–514. CrossRef Medline

Colbran RJ (2004) Protein phosphatases and calcium/calmodulin-dependent protein kinase II-dependent synaptic plasticity. J Neurosci 24:8404–8409. CrossRef Medline

Cummings DM, André VM, Uzgil BO, Gee SM, Fisher YE, Cepeda C, Levine MS (2009) Alterations in cortical excitation and inhibition in genetic mouse models of Huntington's disease. J Neurosci 29:10371–10386. CrossRef Medline

Decavel C, Van den Pol AN (1990) GABA: a dominant neurotransmitter in the hypothalamus. J Comp Neurol 302:1019–1037. CrossRef Medline

Eckstein F (1985) Nucleoside phosphorothioates. Annu Rev Biochem 54: 367–402. CrossRef Medline

Fáncsik A, Linn DM, Tasker JG (2000) Neurosteroid modulation of GABA IPSCs is phosphorylation dependent. J Neurosci 20:3067–3075. Medline

Fleming TM, Scott V, Naskar K, Joe N, Brown CH, Stern JE (2011) State-dependent changes in astrocyte regulation of extrasynaptic NMDA receptor signalling in neurosecretory neurons. J Physiol 589:3929–3941. Medline

Gaiarsa JL, Caillard O, Ben-Ari Y (2002) Long-term plasticity at GABAergic and glycinergic synapses: mechanisms and functional significance. Trends Neurosci 25:564–570. CrossRef Medline

Goldsmith SR, Francis GS, Cowley AW Jr (1986) Arginine vasopressin and the renal response to water loading in congestive heart failure. Am J Cardiol 58:295–299. CrossRef Medline

Han TH, Lee K, Park JB, Ahn D, Park JH, Kim DY, Stern JE, Lee SY, Ryu PD (2010) Reduction in synaptic GABA release contributes to target-selective elevation of PVN neuronal activity in rats with myocardial infarction. Am J Physiol Regul Integr Comp Physiol 299:R129–R139. CrossRef Medline

Hardingham GE, Bading H (2010) Synaptic versus extrasynaptic NMDA receptor signalling: implications for neurodegenerative disorders. Nat Rev Neurosci 11:682–696. CrossRef Medline

Hu B, Bourque CW (1992) NMDA receptor-mediated rhythmic bursting activity in rat supraoptic nucleus neurones in vitro. J Physiol 458:667–687. Medline

Ishihara H, Martin BL, Brautigan DL, Karaki H, Ozaki H, Kato Y, Fusetani N, Watabe S, Hashimoto K, Uemura D. (1989) Calyculin A and okadaic acid: inhibitors of protein phosphatase activity. Biochem Biophys Res Commun 159:871–877. CrossRef Medline

Jones MV, Westbrook GL (1997) Shaping of IPSCs by endogenous calcineurin activity. J Neurosci 17:7626–7633. Medline

Kang YM, He RL, Yang LM, Qin DN, Guggilam A, Elks C, Yan N, Guo Z, Francis J (2009) Brain tumour necrosis factor-alpha modulates neurotransmitters in hypothalamic paraventricular nucleus in heart failure. Cardiovasc Res 83:737–746. CrossRef Medline

Kano M, Rexhausen U, Dreessen J, Konnerth A (1992) Synaptic excitation produces a long-lasting rebound potentiation of inhibitory synaptic signals in cerebellar Purkinje cells. Nature 356:601–604. CrossRef Medline

Kawaguchi SY, Hirano T (2002) Signaling cascade regulating long-term potentiation of GABA$_A$ receptor responsiveness in cerebellar Purkinje neurons. J Neurosci 22:3969–3976. Medline

Kehrer C, Maziashvili N, Dugladze T, Gloveli T (2008) Altered excitatory-inhibitory balance in the NMDA-hypofunction model of schizophrenia. Front Mol Neurosci 1:6. Medline

Kleiber AC, Zheng H, Schultz HD, Peuler JD, Patel KP (2008) Exercise training normalizes enhanced glutamate-mediated sympathetic activation from the PVN in heart failure. Am J Physiol Regul Integr Comp Physiol 294:R1863–R1872. CrossRef Medline

Krishek BJ, Xie X, Blackstone C, Huganir RL, Moss SJ, Smart TG (1994) Regulation of GABAA receptor function by protein kinase C phosphorylation. Neuron 12:1081–1095. CrossRef Medline

Le Meur K, Galante M, Angulo MC, Audinat E (2007) Tonic activation of NMDA receptors by ambient glutamate of non-synaptic origin in the rat hippocampus. J Physiol 580:373–383. Medline

Li YF, Cornish KG, Patel KP (2003) Alteration of NMDA NR1 receptors

within the paraventricular nucleus of hypothalamus in rats with heart failure. Circ Res 93:990–997. CrossRef Medline

Li YF, Jackson KL, Stern JE, Rabeler B, Patel KP (2006) Interaction between glutamate and GABA systems in the integration of sympathetic outflow by the paraventricular nucleus of the hypothalamus. Am J Physiol Heart Circ Physiol 291:H2847–2856. CrossRef Medline

Lu YM, Mansuy IM, Kandel ER, Roder J (2000) Calcineurin-mediated LTD of GABAergic inhibition underlies the increased excitability of CA1 neurons associated with LTP. Neuron 26:197–205. CrossRef Medline

Marsden KC, Beattie JB, Friedenthal J, Carroll RC (2007) NMDA receptor activation potentiates inhibitory transmission through GABA receptor-associated protein-dependent exocytosis of GABA$_A$ receptors. J Neurosci 27:14326–14337. CrossRef Medline

Mitchell SJ, Silver RA (2000) Glutamate spillover suppresses inhibition by activating presynaptic mGluRs. Nature 404:498–502. CrossRef Medline

Morishita W, Sastry BR (1996) Postsynaptic mechanisms underlying long-term depression of GABAergic transmission in neurons of the deep cerebellar nuclei. J Neurophysiol 76:59–68. Medline

Nicholson R, Spanswick D, Lee K (2004) Nitric oxide inhibits NMDA currents in a subpopulation of substantia gelatinosa neurons of the adult rat spinal cord. Neurosci Lett 359:180–184. CrossRef Medline

Nissen R, Hu B, Renaud LP (1995) Regulation of spontaneous phasic firing of rat supraoptic vasopressin neurones in vivo by glutamate receptors. J Physiol 484:415–424. Medline

Oliet SH, Piet R, Poulain DA (2001) Control of glutamate clearance and synaptic efficacy by glial coverage of neurons. Science 292:923–926. CrossRef Medline

Packer M (1988) Neurohormonal interactions and adaptations in congestive heart failure. Circulation 77:721–730. CrossRef Medline

Packer M, Lee WH, Kessler PD, Gottlieb SS, Bernstein JL, Kukin ML (1987) Role of neurohormonal mechanisms in determining survival in patients with severe chronic heart failure. Circulation 75:IV80–IV92. Medline

Park JB, Skalska S, Stern JE (2006) Characterization of a novel tonic gamma-aminobutyric acidA receptor-mediated inhibition in magnocellular neurosecretory neurons and its modulation by glia. Endocrinology 147:3746–3760. CrossRef Medline

Patel KP (2000) Role of paraventricular nucleus in mediating sympathetic outflow in heart failure. Heart Fail Rev 5:73–86. CrossRef Medline

Patel KP, Zheng H (2012) Central neural control of sympathetic nerve activity in heart failure following exercise training. Am J Physiol Heart Circ Physiol 302:H527–H537. CrossRef Medline

Patel KP, Zhang PL, Krukoff TL (1993) Alterations in brain hexokinase activity associated with heart failure in rats. Am J Physiol 265:R923–R928. Medline

Patel KP, Zhang K, Kenney MJ, Weiss M, Mayhan WG (2000) Neuronal expression of Fos protein in the hypothalamus of rats with heart failure. Brain Res 865:27–34. CrossRef Medline

Piet R, Vargová L, Syková E, Poulain DA, Oliet SH (2004) Physiological contribution of the astrocytic environment of neurons to intersynaptic crosstalk. Proc Natl Acad Sci U S A 101:2151–2155. CrossRef Medline

Poisbeau P, Cheney MC, Browning MD, Mody I (1999) Modulation of synaptic GABA$_A$ receptor function by PKA and PKC in adult hippocampal neurons. J Neurosci 19:674–683. Medline

Potapenko ES, Biancardi VC, Florschutz RM, Ryu PD, Stern JE (2011) Inhibitory-excitatory synaptic balance is shifted toward increased excitation in magnocellular neurosecretory cells of heart failure rats. J Neurophysiol 106:1545–1557. CrossRef Medline

Potapenko ES, Biancardi VC, Zhou Y, Stern JE (2012) Altered astrocyte glutamate transporter regulation of hypothalamic neurosecretory neurons in heart failure rats. Am J Physiol Regul Integr Comp Physiol 303: R291–R300. CrossRef Medline

Randle JC, Renaud LP (1987) Actions of gamma-aminobutyric acid in rat supraoptic nucleus neurosecretory neurons in vitro. J Physiol 387:629–647. Medline

Semyanov A, Kullmann DM (2000) Modulation of GABAergic signaling among interneurons by metabotropic glutamate receptors. Neuron 25: 663–672. CrossRef Medline

Sonner PM, Lee S, Ryu PD, Lee SY, Stern JE (2011) Imbalanced K+ and Ca2+ subthreshold interactions contribute to increased hypothalamic presympathetic neuronal excitability in hypertensive rats. J Physiol 589: 667–683. CrossRef Medline

Stern JE (2001) Electrophysiological and morphological properties of preautonomic neurones in the rat hypothalamic paraventricular nucleus. J Physiol 537:161–177. CrossRef Medline

Stern JE, Ludwig M (2001) NO inhibits supraoptic oxytocin and vasopressin neurons via activation of GABAergic synaptic inputs. Am J Physiol Regul Integr Comp Physiol 280:R1815–R1822. Medline

Sun B, Halabisky B, Zhou Y, Palop JJ, Yu G, Mucke L, Gan L (2009) Imbalance between GABAergic and glutamatergic transmission impairs adult neurogenesis in an animal model of Alzheimer's disease. Cell Stem Cell 5:624–633. CrossRef Medline

Ueta Y, Fujihara H, Serino R, Dayanithi G, Ozawa H, Matsuda K, Kawata M, Yamada J, Ueno S, Fukuda A, Murphy D (2005) Transgenic expression of enhanced green fluorescent protein enables direct visualization for physiological studies of vasopressin neurons and isolated nerve terminals of the rat. Endocrinology 146:406–413. Medline

Vahid-Ansari F, Leenen FH (1998) Pattern of neuronal activation in rats with CHF after myocardial infarction. Am J Physiol 275:H2140–H2146. Medline

van den Pol AN, Wuarin JP, Dudek FE (1990) Glutamate, the dominant excitatory transmitter in neuroendocrine regulation. Science 250:1276–1278. CrossRef Medline

Vogt KE, Nicoll RA (1999) Glutamate and gamma-aminobutyric acid mediate a heterosynaptic depression at mossy fiber synapses in the hippocampus. Proc Natl Acad Sci U S A 96:1118–1122. CrossRef Medline

Wang JH, Stelzer A (1996) Shared calcium signaling pathways in the induction of long-term potentiation and synaptic disinhibition in CA1 pyramidal cell dendrites. J Neurophysiol 75:1687–1702. Medline

Yang Z, Coote JH (1998) Influence of the hypothalamic paraventricular nucleus on cardiovascular neurones in the rostral ventrolateral medulla of the rat. J Physiol 513:521–530. CrossRef Medline

Zhang K, Li YF, Patel KP (2001) Blunted nitric oxide-mediated inhibition of renal nerve discharge within PVN of rats with heart failure. Am J Physiol Heart Circ Physiol 281:H995–1004. Medline

Zhang K, Li YF, Patel KP (2002) Reduced endogenous GABA-mediated inhibition in the PVN on renal nerve discharge in rats with heart failure. Am J Physiol Regul Integr Comp Physiol 282:R1006–R1015. Medline

Zheng H, Liu X, Li Y, Sharma NM, Patel KP (2011) Gene transfer of neuronal nitric oxide synthase to the paraventricular nucleus reduces the enhanced glutamatergic tone in rats with chronic heart failure. Hypertension 58:966–973. CrossRef Medline